Mechanochemically driven solid-state Diels–Alder reaction of graphite into graphene nanoplatelets†

Jeong-Min Seo, In-Yup Jeon and Jong-Beom Baek*

A mechanochemically driven solid-state Diels–Alder reaction is demonstrated *via* dry ball-milling graphite as the diene in the presence of maleic anhydride or maleimide as the dienophile. On the basis of various characterizations, the Diels–Alder adducts are edge-selectively functionalized and subsequently delaminated into graphene nanoplatelets.

Introduction

Since buckminsterfullerene was discovered in the mid-1980s,[1–3] synthetic carbon nanomaterials have enriched materials research. What makes carbon nanomaterials so attractive for chemists, physicists, and material scientists is not only their aesthetic structure but, even more so, their outstanding and unprecedented new properties.[4,5] Arising from their fully conjugated fused aromatic network structures,[6] they have chemical stability, which has been both an advantage and a disadvantage. The intrinsic chemical inertness results in a lack of processability, which is a prerequisite for their use in most technological applications. To enable the processing of carbon nanomaterials, chemical modification has attracted a lot of attention as a way to make carbon nanomaterials processable and therefore useful in practice.[7]

Hitherto, various methods for the functionalization of carbon nanomaterials have been devised including radical addition,[8,9] cycloaddition,[10,11] hydrogenation,[12,13] and fluorination.[14,15] Among them, the Diels–Alder reaction, *i.e.*, [4 + 2] cycloaddition, is one of the most viable synthetic protocols for carbon nanomaterials, because a wide variety of functional groups can be introduced. In contrast to fullerene and carbon nanotubes, which always act as the dienophile in [4 + 2] cycloaddition due to their curvatures,[16,17] 2-dimensional graphene and its derivatives are able to behave as both diene and dienophile.[18,19] Based on this hypothesis, Haddon, *et al.*, reported the Diels–Alder reaction of graphene on its basal plane by heating of graphite and dienophile.[18] For thermal reaction in solution, a rather large amount of solvent is usually required due to the poor solubility of graphite in common organic solvents. Consequently, solution-based Diels–Alder reaction results in a low degree of functionalization with poor yield.[20] As an alternative method for solution-based synthesis, solvent-free synthesis of carbon nanomaterials has been proposed to overcome this difficulty.[21] On the basis of our previous works on the mechanochemical modifications of graphite *via* dry ball-milling in the presence of dry ice[22] and reactive gases,[23] here, for the first time, we report solid-state [4 + 2] cycloaddition between graphite and dienophile. Graphite was selected as a diene, and maleic anhydride (MA) and maleimide (MI) were chosen as dienophiles to ensure feasibility. Compared with many previous methods, the approach applied in this work is simple but efficient to produce edge-selectively functionalized graphene nanoplatelets (EFGnPs). The resultant EFGnPs are highly dispersible in various polar solvents, including water. Furthermore, each EFGnP shows different dispersibility depending on the nature of the functional groups.

Experimental section

Materials

Graphite (natural, 100 mesh, <150 μm, 99.9995% metal basis, Lot no. 14375) was obtained from Alfa Aesar. Maleic anhydride (FW = 98.06) and maleimide (FW = 97.07) were purchased from Sigma Aldrich Chemical Inc. and used as received.

Synthesis of MA-GnPs and MI-GnPs by ball-milling

In a typical experiment, pristine graphite (5 g) and maleic anhydride (10 g, 0.102 mol) or maleimide (10 g, 0.103 mol) were placed into a stainless steel container with stainless steel balls (500 g, 5 mm in diameter). The container was sealed and 5 cycles of argon gas charge/discharge were applied. The container was then fixed in the planetary ball-mill machine (Pulverisette 6, Fritsch) and agitated at 500 rpm for 48 h. Thereafter the resultant products were stirred with 1 M aqueous HCl solution to completely acidify the residual active species and to remove metallic impurities, if any. Further Soxhlet extractions were conducted with THF and water for 72 h and 48 h, respectively, and freeze-dried at −120 °C under a reduced

Ulsan National Institute of Science and Technology (UNIST), Interdisciplinary School of Green Energy/Low-Dimensional Carbon Materials Center, 100 Banyeon, Ulsan 689-798, South Korea. E-mail: jbbaek@unist.ac.kr; Fax: +82-52-217-2019; Tel: +82-52-217-2510

pressure (0.05 mmHg) for 48 h to yield 6.45 g of MA-GnPs and 7.09 g of MI-GnPs as a dark-black powder. Found for MA-GnPs: C: 86.10%; H: 1.07%; O: 10.10%. Found for MI-GnPs: 84.97%; H: 1.21%; O: 8.91%; N: 3.06%.

Instrumentation

Fourier transform infrared (FT-IR) spectra were recorded on a Perkin-Elmer Spectrum 100 using KBr pellets. Thermogravimetric analysis (TGA) measurements were carried out using a TA Q200 with a heating rate of 10 °C min^{-1} in air and nitrogen. The morphology of the as-prepared samples was examined by field-emission scanning electron microscopy (FE-SEM, FEI Nanonova 230). Elemental analysis (EA) was conducted on a Thermo Scientific Flash 2000. X-ray photoelectron spectra (XPS) were recorded on a Thermo Fisher K-alpha XPS spectrometer. Raman spectra were recorded using an Alpha 300S confocal Raman spectrometer (WITec, Germany) with a 532 nm He–Ne laser. Contact angle measurements were conducted on a Krüss DSA 100 contact angle analyzer. Sample solutions were coated on a silicon (Si) wafer.

Results and discussion

Synthesis of edge-selectively functionalized graphene nanoplatelets (EF-GnPs)

MA- (MA-GnPs) and MI-functionalized graphene nanoplatelets (MI-GnPs) were prepared by [4 + 2] cycloaddition *via* ball-milling of graphite in the presence of MA or MI, respectively, as a corresponding dienophile (Fig. 1a). Large pieces of pristine graphite flake (100 mesh, >150 μm, Fig. 1b) were readily crushed into small grain sizes of graphene nanoplatelets (GnPs) (Fig. 1c and d), suggesting that the mechanochemically driven reaction by ball-milling should lead to changes in the morphologies of the resultant edge-selectively functionalized GnPs (EFGnPs). The grain sizes of the resultant EFGnPs were dramatically reduced to the range of 0.1–1 μm, compared with pristine graphite. This result implies that mechanochemical ball-milling effectively promotes C–C bond breaking, functionalization, and subsequent delamination of graphite into GnPs. The kinetic energy of high-speed steel balls cracks the graphitic C–C bonds and generates reactive carbon species. It is known that reactive carbon species are mostly radicals due to homolytic cleavages and ions (cations and anions) due to heterolytic cleavages along the broken edges,[22] which may lead to efficient promotion of [4 + 2] cycloaddition. On the basis of perylene as a miniature model compound for graphite, it is known that [4 + 2] cycloaddition occurs at the bay region of perylene, which, in turn, implies that [4 + 2] cycloaddition reacts at the armchair edges of graphite.[24] Therefore, cycloaddition is expected to occur more along armchair edges rather than zigzag edges and the graphitic basal plane in the presence of MA or MI as dienophile (see Fig. 1a and Fig. S1 in, ESI†). The rest of the remnant active carbon species at the armchair and zigzag edges could be terminated by exposure to air moisture. As a result, some oxygenated groups, such as hydroxyl (–OH) and carboxylic (–COOH) groups should also be introduced at the cracked edges
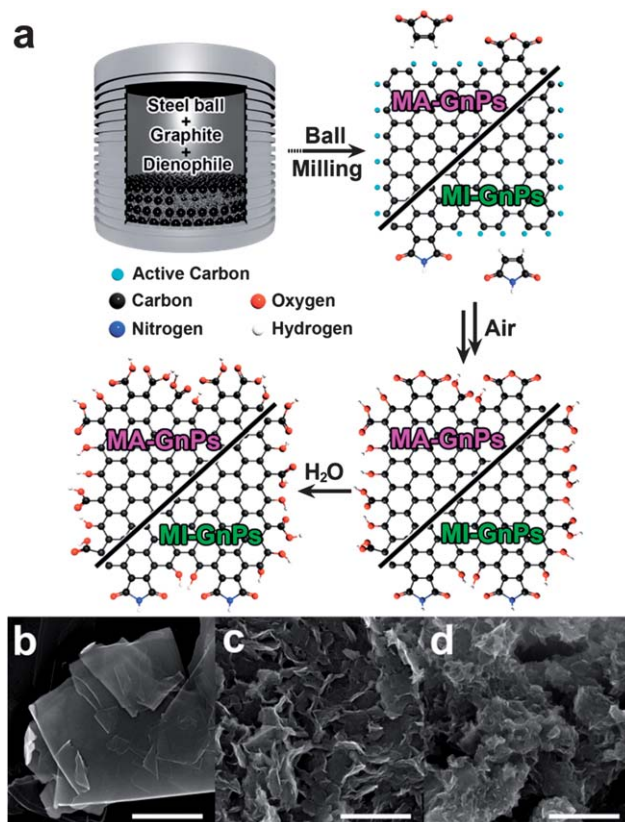
Fig. 1 (a) Schematic representation of the mechanochemically driven solid-state Diels–Alder reaction between *in situ* generated active carbon species by ball-milling in the presence of a specific dienophile, maleic anhydride (MA) or maleimide (MI). Active carbon species along the broken edges would more efficiently promote [4 + 2] cycloaddition, and the remnant should be terminated by subsequent exposure to air moisture, forming oxygenated groups. The anhydride moieties at the edges of MA-GnPs could be hydrolyzed into carboxylic acids during acid-mediated work-up procedures. SEM images: (b) pristine graphite, (c) MA-GnPs, (d) MI-GnPs. Scale bars are 1 μm.

of the resultant EFGnPs (Fig. 1a).[23] The weight increased in both MA-GnPs and MI-GnPs after mechanochemical ball-milling, and complete work-up procedures showed evidence of the weight-gaining functionalization *via* solid-state Diels–Alder reaction (see Experimental section). Elemental analysis (EA) showed that MA-GnPs and MI-GnPs have the carbon contents of 86.10% and 84.97%, respectively, and oxygen contents of 10.10% and 8.91%, respectively (Table S1†), while pristine graphite has carbon and oxygen contents of 97.71% and below the detection limit, respectively. Furthermore, only MI-GnPs have a nitrogen content of 3.06%. The results indicate that new elements were introduced to the GnPs. The sole presence of nitrogen in MI-GnPs was further confirmed by SEM element mapping with an energy dispersive spectrometer (EDS) of the samples (Fig. S2 and Table S2†).

Although MA and MI have similar structures (Fig. S1†), the resultant MA-GnPs and MI-GnPs are expected to possess different properties owing to the differences in the chemical nature of the final structures. After stirring in 1 M aq. HCl solution to eliminate residual metallic impurities, if any, and further Soxhlet extraction with water (see Experimental section),

the anhydride moieties at the edges of MA-GnPs were expected to be hydrolyzed into carboxylic acids, while the imide rings of MI-GnPs are relatively stable and thus remain intact.[25,26] Consequently, the difference in polarity between open-shaped carboxylic acids and close-shaped imide rings should display different dispersibility in polar solvents (*vide infra*).

Characterization of MA-GnPs and MI-GnPs

To further quantitatively and qualitatively identify Diels–Alder reaction adducts, thermogravimetric analysis (TGA), Fourier transform infrared (FT-IR) and X-ray photoelectron spectroscopy (XPS) were used. Compared with pristine graphite, the TGA thermograms of MA-GnPs and MI-GnPs obtained show that gradual weight loss started from the beginning and the measured values were approximately 14% and 18% at around 435 °C and 540 °C in air, respectively (Fig. S3a†). The char yields of MA-GnPs and MI-GnPs were 15.1% and 17.6%, respectively, at 1000 °C in nitrogen (Fig. S3b†). The early weight loss of EFGnPs is attributed to the thermal decomposition of edge functional groups.[22]

The types of functional groups at the edges of the resultant EFGnPs can be confirmed by FT-IR spectroscopy and XPS. While pristine graphite shows an almost featureless FT-IR spectrum (Fig. 2a), MA-GnPs and MI-GnPs display a strong band at 1582 cm^{-1}, which is attributable to the C=C stretching band at the edges of EFGnPs. Both samples also exhibit similar bands at around 1200 and 3400 cm^{-1}, respectively, corresponding to C–O and O–H stretching attributed to carboxylic or hydroxyl groups at the edges. In the case of MI-GnPs, overlapping between O–H and N–H stretching may occur at around 3400 cm^{-1}. MA-GnPs and MI-GnPs have the same band, which appears at 1711 cm^{-1} and is attributed to C=O stretching. N–H bending overlapped with C=O stretching. In addition, MI-GnPs display a small band at 1345 cm^{-1}, which is attributed to C–N stretching from maleimide ring moieties at the edges. The results suggest that anhydride groups (mostly C=O stretching in anhydride appears at 1830 cm^{-1}) on MA-GnPs are hydrolyzed into carboxylic acids,[27] whereas the maleimide rings on MI-GnPs remain intact during acid-mediated work-up procedures.[25,26]

For more detailed analysis, both EFGnPs were further examined by XPS (Fig. 2b, S4 and Table S2†). While pristine graphite shows a very minor O 1s peak at 532 eV relative to the C 1s peak at 284 eV due to physically adsorbed oxygen,[28,29] MA-GnPs and MI-GnPs display relative strong O 1s peaks owing to the edge functional groups (Fig. 2b). The high-resolution XPS surveys with curve fitting of O 1s spectra of both MA-GnPs and MI-GnPs reveal that the O element is assignable to C–O and C=O bonding (Fig. S4b and d in ESI†), which are associated with C–OH, O=C–OH, and O=C–N–C=O moieties. Once again, the N 1s peak at 400 eV, which corresponds to pyrrolic-N of the imide ring (inset, Fig. 2b),[30,31] was only observed with MI-GnPs.

The Raman spectra of edge-selective [4 + 2] cycloadditions *via* ball-milling graphite in the presence of dienophile which exclusively occurred at the edges were obtained from the edges and basal areas of samples with a focused laser beam.
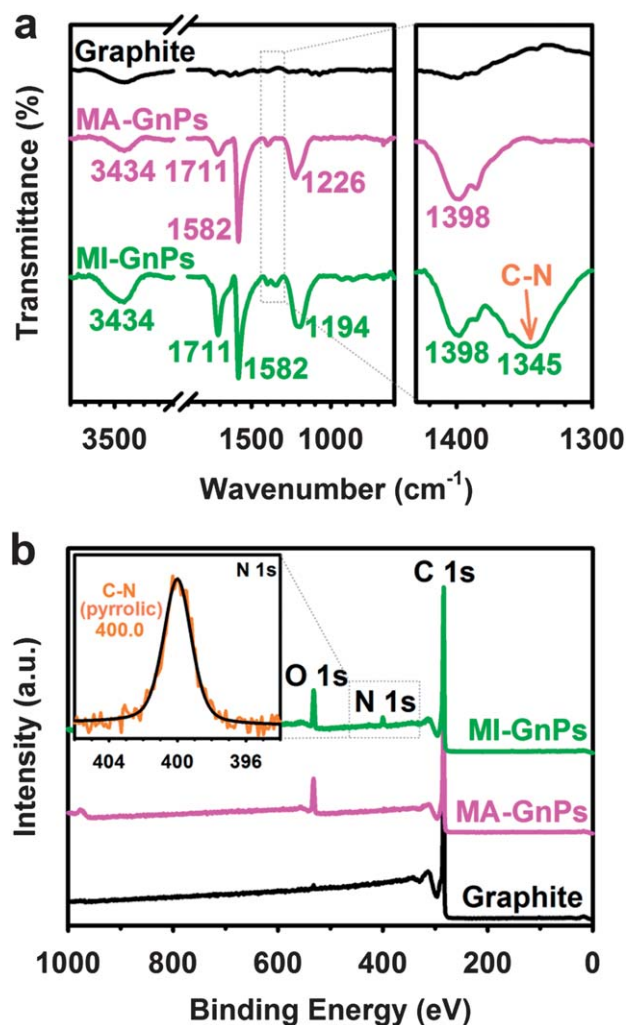
Fig. 2 (a) Full FT-IR spectra (KBr pellets) (left) and magnified spectra (right); (b) XPS survey spectra. Inset: high-resolution XPS N 1s spectrum of MI-GnPs.

The Raman spectrum obtained from the edge area of pristine graphite shows a strong G band at 1580 cm^{-1} and a 2D band at 2717 cm^{-1} with a very weak D band at 1350 cm^{-1} (Fig. 3a), indicating a highly ordered structure with low defects. Pristine graphite has the ratio of the D- to G-band intensities (I_D/I_G) of only 0.01. However, MA-GnPs and MI-GnPs have much stronger D-bands at 1350 cm^{-1}, stemming from a high degree of edge distortion by functionalization along with size reduction. As a result, the I_D/I_G ratios of MA-GnPs and MI-GnPs are 0.62 and 1.04, respectively. The Raman spectrum obtained from the basal area of the starting graphite shows strong G and 2D peaks without a detectable D peak, whereas those of MA-GnPs and MI-GnPs have detectable D peaks (Fig. 3b).[32] However, the I_D/I_G ratios of MA-GnPs and MI-GnPs were 0.04 and 0.40, respectively, which are relatively much lower than those obtained from edge areas. Note that the grain sizes of both EFGnPs are significantly smaller than pristine graphite as seen in Fig. 1b–d. The relatively smaller D-bands from MA-GnPs and MI-GnPs are most likely contributed by edges, because the wavelength (532 nm) of the Raman laser is similar to the grain sizes of EFGnPs.[33] Thus,
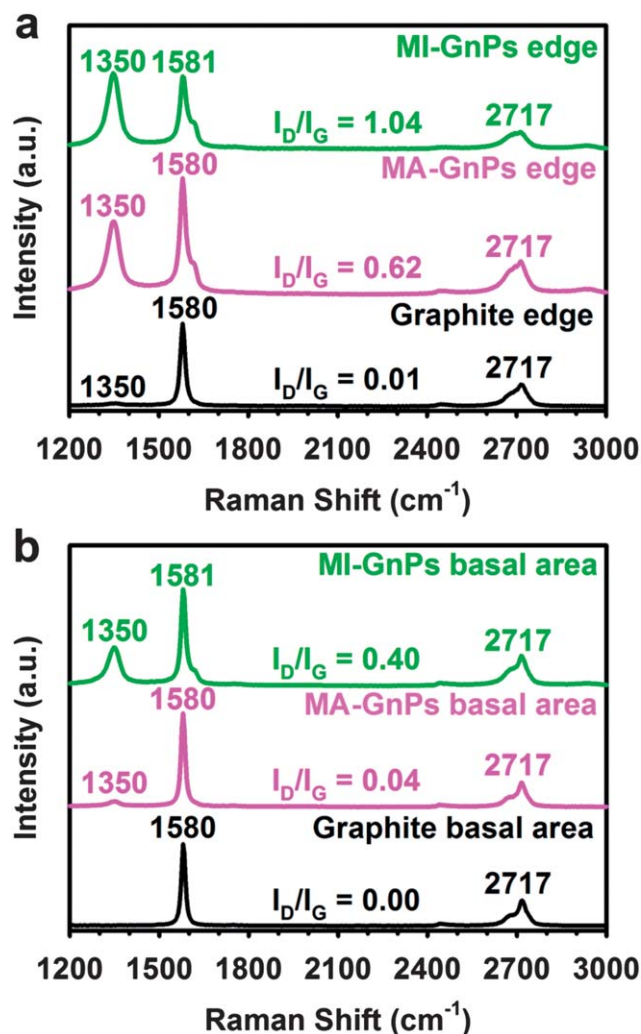
Fig. 3 Raman spectra obtained by a focused laser: (a) edge area and (b) basal area.

Fig. 4 Photographs of sample dispersion in ethanol after 3 months standing under normal laboratory conditions: (a) MA-GnPs and (b) MI-GnPs. Concentration is 0.3 mg ml^{-1}. Photographs of sample dispersion in water after 3 months standing under normal laboratory conditions: (c) MA-GnPs and (d) MI-GnPs. Concentration is 0.3 mg ml^{-1}. Contact angle images of samples: (e) MA-GnPs and (f) MI-GnPs.

EFGnP-coated silicon substrates. MA-GnPs show a lower water contact angle (45.1°) (Fig. 4e) than MI-GnPs (67.9°) (Fig. 4f), indicating the higher surface polarity of MA-GnPs (Table S3†).

Conclusions

In summary, for the first time, we have demonstrated the solid-state Diels–Alder reaction of graphite. Mechanochemical ball-milling breaks the graphitic C–C bonds and generates active carbon species (mostly carboradicals, carboanions and carbo-cations), which couple with a dienophile, such as maleic anhydride or maleimide. The resultant edge-selectively functionalized graphene nanoplatelets were readily dispersible in various solvents. Hence, considering the availability of dien-ophiles, the Diels–Alder reaction *via* ball-milling graphite could be a general method for the chemical modification of graphite into graphene nanoplatelets.

Acknowledgements

Notes and references

1 H. W. Kroto, J. R. Heath, S. C. Obrien, R. F. Curl and R. E. Smalley, *Nature*, 1985, **318**, 162–163.
2 S. Iijima, *Nature*, 1991, **354**, 56–58.
3 K. S. Novoselov, A. K. Geim, S. V. Morozov, D. Jiang, Y. Zhang, S. V. Dubonos, I. V. Grigorieva and A. A. Firsov, *Science*, 2004, **306**, 666–669.
4 M. J. Allen, V. C. Tung and R. B. Kaner, *Chem. Rev.*, 2010, **110**, 132–145.
5 A. Hirsch, J. M. Englert and F. Hauke, *Acc. Chem. Res.*, 2013, **46**, 87–96.

the Raman results indicate that the [4 + 2] cycloadditions almost exclusively occurred at the edges of EFGnPs.

The edge-functionalization of GnPs is expected to lead to improved dispersibility due to the edge functionality (enthalpic gains) and size reduction (entropic gains), which should provide the thermodynamic driving force for dispersion in various solvents. Thus, EFGnPs can disperse well in most protic and polar aprotic solvents, including neutral water.[23] For example, both EFGnPs show good dispersibility in ethanol (Fig. 4a and b) and other protic and polar aprotic solvents (Fig. S5 in ESI†). However, they display clearly different dispersion stability in H$_2$O, as shown in Fig. 4c and d, indicating that MA-GnPs have better dispersion stability than MI-GnPs in water. It is likely due to the hydrogen bonding between water molecules and carboxylic acid groups at the edges of MA-GnPs. The variation in dispersibility supports the hydrolysis of anhy-dride into carboxylic acids in MA-GnPs. For further evidence, contact angle measurements could distinguish the differences between the surface polarities of MA-GnPs and MI-GnPs, which were performed by placing droplets of de-ionized water on
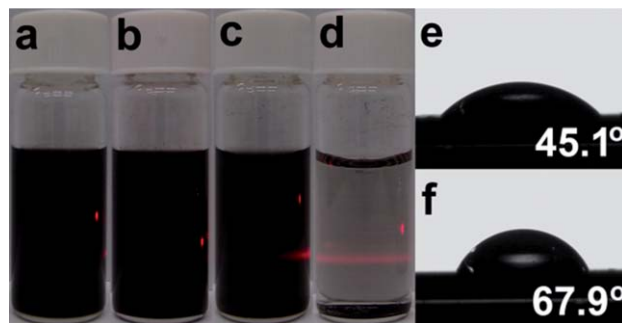
6 A. Hirsch, *Nat. Mater.*, 2010, **9**, 868–871.

7 V. Georgakilas, M. Otyepka, A. B. Bourlinos, V. Chandra, N. Kim, K. C. Kemp, P. Hobza, R. Zboril and K. S. Kim, *Chem. Rev.*, 2012, **112**, 6156–6214.

8 J. L. Bahr, J. P. Yang, D. V. Kosynkin, M. J. Bronikowski, R. E. Smalley and J. M. Tour, *J. Am. Chem. Soc.*, 2001, **123**, 6536–6542.

9 A. Sinitskii, A. Dimiev, D. A. Corley, A. A. Fursina, D. V. Kosynkin and J. M. Tour, *ACS Nano*, 2010, **4**, 1949–1954.

10 V. Georgakilas, K. Kordatos, M. Prato, D. M. Guldi, M. Holzinger and A. Hirsch, *J. Am. Chem. Soc.*, 2002, **124**, 760–761.

11 V. Georgakilas, A. B. Bourlinos, R. Zboril, T. A. Steriotis, P. Dallas, A. K. Stubos and C. Trapalis, *Chem. Commun.*, 2010, **46**, 1766–1768.

12 K. S. Kim, D. J. Bae, J. R. Kim, K. A. Park, S. C. Lim, J. J. Kim, W. B. Choi, C. Y. Park and Y. H. Lee, *Adv. Mater.*, 2002, **14**, 1818–1821.

13 S. Ryu, M. Y. Han, J. Maultzsch, T. F. Heinz, P. Kim, M. L. Steigerwald and L. E. Brus, *Nano Lett.*, 2008, **8**, 4597–4602.

14 E. T. Mickelson, C. B. Huffman, A. G. Rinzler, R. E. Smalley, R. H. Hauge and J. L. Margrave, *Chem. Phys. Lett.*, 1998, **296**, 188–194.

15 J. T. Robinson, J. S. Burgess, C. E. Junkermeier, S. C. Badescu, T. L. Reinecke, F. K. Perkins, M. K. Zalalutdniov, J. W. Baldwin, J. C. Culbertson, P. E. Sheehan and E. S. Snow, *Nano Lett.*, 2010, **10**, 3001–3005.

16 A. Krueger, in *Carbon Materials and Nanotechnology*, Wiley-VCH Verlag GmbH & Co. KGaA, 2010, pp. 33–122.

17 A. Krueger, in *Carbon Materials and Nanotechnology*, Wiley-VCH Verlag GmbH & Co. KGaA, 2010, pp. 123–281.

18 S. Sarkar, E. Bekyarova, S. Niyogi and R. C. Haddon, *J. Am. Chem. Soc.*, 2011, **133**, 3324–3327.

19 S. Sarkar, E. Bekyarova and R. C. Haddon, *Acc. Chem. Res.*, 2012, **45**, 673–682.

20 Y. Murata, N. Kato, K. Fujiwara and K. Komatsu, *J. Org. Chem.*, 1999, **64**, 3483–3488.

21 A. Stolle, T. Szuppa, S. E. S. Leonhardt and B. Ondruschka, *Chem. Soc. Rev.*, 2011, **40**, 2317–2329.

22 I. Y. Jeon, Y. R. Shin, G. J. Sohn, H. J. Choi, S. Y. Bae, J. Mahmood, S. M. Jung, J. M. Seo, M. J. Kim, D. W. Chang, L. M. Dai and J. B. Baek, *Proc. Natl. Acad. Sci. U. S. A.*, 2012, **109**, 5588–5593.

23 I. Y. Jeon, H. J. Choi, S. M. Jung, J. M. Seo, M. J. Kim, L. M. Dai and J. B. Baek, *J. Am. Chem. Soc.*, 2013, **135**, 1386–1393.

24 E. Clar and M. Zander, *J. Chem. Soc.*, 1957, 4616–4619.

25 M. N. Khan, *J. Pharm. Sci.*, 1984, **73**, 1767–1771.

26 H. Kwart and I. Burchuk, *J. Am. Chem. Soc.*, 1952, **74**, 3094–3097.

27 B. Schneider, O. D. Hennemann and W. Possart, *J. Adhes.*, 2002, **78**, 779–797.

28 H. Ulbricht, G. Moos and T. Hertel, *Phys. Rev. B: Condens. Matter*, 2002, **66**, 075404.

29 P. Giannozzi, R. Car and G. Scoles, *J. Chem. Phys.*, 2003, **118**, 1003–1006.

30 Y. Wang, Y. Y. Shao, D. W. Matson, J. H. Li and Y. H. Lin, *ACS Nano*, 2010, **4**, 1790–1798.

31 Z. H. Sheng, L. Shao, J. J. Chen, W. J. Bao, F. B. Wang and X. H. Xia, *ACS Nano*, 2011, **5**, 4350–4358.

32 A. C. Ferrari, *Solid State Commun.*, 2007, **143**, 47–57.

33 C. J. Shih, A. Vijayaraghavan, R. Krishnan, R. Sharma, J. H. Han, M. H. Ham, Z. Jin, S. C. Lin, G. L. C. Paulus, N. F. Reuel, Q. H. Wang, D. Blankschtein and M. S. Strano, *Nat. Nanotechnol.*, 2011, **6**, 439–445.